

1 **Increased Importance of Aerosol-Cloud Interaction for Surface**  
2 **PM<sub>2.5</sub> Pollution Relative to Aerosol-Radiation Interaction in**  
3 **China with the Anthropogenic Emission Reduction**

Deleted: W

4  
5 Da Gao<sup>1, 2</sup>, Bin Zhao<sup>1, 2, \*</sup>, Shuxiao Wang<sup>1, 2</sup>, Yuan Wang<sup>3</sup>, Brian Gaudet<sup>4</sup>, Yun  
6 Zhu<sup>5</sup>, Xiaochun Wang<sup>1, 2</sup>, Jiewen Shen<sup>1, 2</sup>, Shengyue Li<sup>1, 2</sup>, Yicong He<sup>1, 2</sup>, Dejie  
7 Yin<sup>1, 2</sup>, Zhaoxin Dong<sup>1, 2</sup>

8  
9 <sup>1</sup>State Key Joint Laboratory of Environment Simulation and Pollution Control,  
10 School of Environment, Tsinghua University, 100084 Beijing, China

11 <sup>2</sup>State Environmental Protection Key Laboratory of Sources and Control of Air  
12 Pollution Complex, Beijing, 100084, China

13 <sup>3</sup>Department of Earth, Atmospheric, and Planetary Sciences, Purdue University,  
14 West Lafayette, IN, USA,

15 <sup>4</sup>Pacific Northwest National Laboratory, Richland, Washington, USA

16 <sup>5</sup>Guangdong Provincial Key Laboratory of Atmospheric Environment and  
17 Pollution Control, College of Environment and Energy, South China University  
18 of Technology, Guangzhou Higher Education Mega Center, Guangzhou, 510006,  
19 China

20 \*Correspondence to: Bin Zhao (bzhao@mail.tsinghua.edu.cn)

21  
22 **Abstract:** Surface fine particulate matter (PM<sub>2.5</sub>) pollution can be enhanced by

24 feedback processes induced by aerosol-radiation interactions (ARI) and aerosol-  
25 cloud interactions (ACI). Many previous studies have reported enhanced PM<sub>2.5</sub>  
26 concentration induced by ARI and ACI for episodic events in China. However,  
27 few studies have examined the changes in the ARI- and ACI-induced PM<sub>2.5</sub>  
28 enhancements over a long period, though the anthropogenic emissions have  
29 changed substantially in the last decade. In this study, we quantify the ARI- and  
30 ACI-induced PM<sub>2.5</sub> changes for 2013–2021 under different meteorology and  
31 emission scenarios using the Weather Research and Forecasting model with  
32 Chemistry (WRF-Chem) and investigate the driving factors for the changes. Our  
33 results show that in January 2013, when China suffered from the worst PM<sub>2.5</sub>  
34 pollution, the PM<sub>2.5</sub> enhancement induced by ARI in eastern China (5.59 μg m<sup>-3</sup>)  
35 is larger than that induced by ACI (3.96 μg m<sup>-3</sup>). However, the ACI-induced  
36 PM<sub>2.5</sub> enhancement shows a significantly smaller decrease ratio (51%) than the  
37 ARI-induced enhancement (75%) for 2013–2021, making ACI more important  
38 for enhancing PM<sub>2.5</sub> concentrations in January 2021. Our analyses suggest that  
39 the anthropogenic emission reduction plays a key role in this shift. Owing to only  
40 anthropogenic emission reduction, the ACI-induced PM<sub>2.5</sub> enhancement  
41 decreases by 43% in January, lower than the decrease ratio of the ARI-induced  
42 enhancement (57%). The relative change in ARI- and ACI-induced PM<sub>2.5</sub>  
43 enhancement in July is similar to the pattern observed in January caused by  
44 anthropogenic emission reduction. The primary reason for this phenomenon is  
45 that the decrease of ambient PM<sub>2.5</sub> for 2013–2021 causes a disproportionately

Deleted: the ACI-induced PM<sub>2.5</sub> enhancement decreases by 43% in January and 57% in July, lower than the decrease ratio of the ARI-induced enhancement (57% in January and 67% in July). ...

50 small decrease of liquid water path (LWP) and increase of cloud effective radius  
51 (Re) under the condition of high PM<sub>2.5</sub> concentration. ~~Therefore,~~ the surface solar  
52 radiation attenuation (and hence boundary layer height reduction) caused by ACI  
53 decreases slower than that caused by ARI. Moreover, the lower decrease ratio of  
54 the ACI-induced PM<sub>2.5</sub> enhancement is dominated by the lower decrease ratio of  
55 ACI-induced secondary PM<sub>2.5</sub> component enhancement, which is additionally  
56 caused by smaller decrease ratio of the air temperature reduction and relative  
57 humidity (RH) increase. Our findings ~~indicate that,~~ with the decrease of ambient  
58 PM<sub>2.5</sub>, the ACI-induced PM<sub>2.5</sub> enhancement inevitably becomes more important.  
59 ~~This~~ needs to be considered in the formulation of control policies to meet the  
60 national PM<sub>2.5</sub> air quality standard.

Deleted: ,

Deleted: t

Deleted:

Deleted: reveal

Deleted: ,

Deleted: which

61

## 62 1. Introduction

63 Aerosol-radiation interaction (ARI) and aerosol-cloud interaction (ACI) are  
64 important ways for aerosols to influence the climate (Rosenfeld et al., 2014;  
65 Seinfeld et al., 2016; Liu et al., 2018; Bellouin et al., 2020; Forster et al., 2021).  
66 The ARI represents the direct scattering and absorption of solar and infrared  
67 radiation by atmospheric aerosols; the ACI denotes the modification effects on  
68 the lifetime, physical and optical properties of clouds by atmospheric aerosols.

69 Previous studies have documented that both ARI and ACI have important  
70 contributions to inhibiting the planetary boundary layer height (PBLH), cooling  
71 the near-surface air temperature, and increasing the relative humidity (RH) (Wang  
72 et al., 2014; Ding et al., 2016; Liu et al., 2018). Moreover, ACI has extra

79 contributions to changing precipitation and cloud chemistry (Zhao et al., 2017;  
80 Zhang et al., 2018). These feedbacks and changes are mostly conducive to  
81 increasing the haze severity (Wang et al., 2015; Zhang et al., 2018; Liu et al.,  
82 2018; Zhou et al., 2019; Zhang et al., 2020; Xiong et al., 2022; Lin et al., 2022).  
83 So far, numerous studies have evaluated the fine particulate matter (PM<sub>2.5</sub>)  
84 enhancements caused by the decreases of downward shortwave radiation at the  
85 surface (SWDOWN), PBLH, near-surface air temperature and precipitation, and  
86 by the increase of RH, especially during the severe PM<sub>2.5</sub> pollution in China (Le  
87 et al., 2020). Zhang et al. (2015) and Zhang et al. (2018) quantified that the ARI  
88 caused the PM<sub>2.5</sub> increase by 8.3  $\mu\text{g m}^{-3}$  in 2013 and 4.0  $\mu\text{g m}^{-3}$  in 2014. However,  
89 both positive and negative contributions of ACI to the PM<sub>2.5</sub> have been revealed  
90 (Forkel et al., 2012; 2015; Kong et al., 2015; Zhang et al., 2015; Zhang et al.,  
91 2018). Zhao et al. (2017) pointed out that the negative contribution of ACI shown  
92 in some studies (Gustafson et al., 2007; Gong et al., 2015) is due to the relatively  
93 high prescribed values of cloud droplet number concentration (CDNC) or cloud  
94 condensation nuclei (CCN), which could not represent a rather clean condition.  
95 Besides, there might be a discrepancy between the enhancements induced by ARI  
96 and ACI for primary and secondary PM<sub>2.5</sub> components. The primary PM<sub>2.5</sub>  
97 components are mainly influenced by physical transport, while the secondary  
98 PM<sub>2.5</sub> components are also affected by chemical formation and decomposition.  
99 The lower air temperature and higher RH can help to condense gas precursors  
100 into secondary aerosol particles (Donahue et al., 2012) and strengthen aqueous

101 and heterogeneous reactions (Liu et al., 2018). On the contrary, Wu et al. (2020)  
102 pointed out that the ARI may also suppress the formation of secondary aerosol  
103 because the atmospheric oxidizing capacity and photolysis rate can be changed  
104 during the scattering and absorbing of solar radiation. Therefore, not all changes  
105 of meteorological factors are conducive to the increase of secondary PM<sub>2.5</sub>, and  
106 these positive and negative contributions would influence the variations of  
107 primary and secondary PM<sub>2.5</sub> components. In a word, although the ARI and ACI  
108 processes mostly lead to a net PM<sub>2.5</sub> increase, the relative increasing rates of  
109 different aerosol components are fairly complex due to various physical and  
110 chemical processes.

111 In recent years, the Chinese government has successively proclaimed the  
112 policies of “Air pollution prevention and control action plan” and “Three-year  
113 action plan to win the blue sky defense war”, including the promotion of ultra-  
114 low emission technologies in industrial sectors, the implementation of traffic  
115 restriction policies, and the transition from coal to gas in residential cooking. As  
116 a result, the annually averaged PM<sub>2.5</sub> concentrations in Beijing-Tianjin-Hebei  
117 region, Yangtze River Delta (YRD) and Pearl River Delta have been reduced by  
118 39.6%, 34.2%, and 27.7% from 2013 to 2017, respectively (Wang et al., 2017;  
119 Ding et al., 2019a). Meanwhile, sulfate and organic components have respectively  
120 decreased by 76% and 70 % in the North China Plain (NCP) (Wang et al., 2019).  
121 Considering the sharp anthropogenic emission reduction and PM<sub>2.5</sub> concentration  
122 decrease, Moch et al. (2022) found that the decrease in mean PM<sub>2.5</sub> concentration

Formatted: First line: 2 ch

Deleted: Moch et al. (2022) found that the decrease of mean PM<sub>2.5</sub> concentration weakened the cloud-snowfall-albedo feedback induced by the aerosol semi-direct effect. For air quality, Zhang et al. (2022) found that the decrease of black carbon (BC) would reduce the enhanced PM<sub>2.5</sub> concentration induced by the ARI by 1.8 μg m<sup>-3</sup> in January and 0.3 μg m<sup>-3</sup> in July.

Formatted: Font: (Default) Times New Roman

130 from the winter months of 2012–2013 to the winter months of 2016–2017 in  
131 China weakened the cloud–snowfall–albedo feedback induced by the aerosol  
132 semi-direct effect. For air quality, Zhang et al. (2022) found that the decrease in  
133 black carbon from 2013 to 2017 in China reduced the enhanced PM<sub>2.5</sub>  
134 concentration induced by the ARI by 1.8 μg m<sup>-3</sup> in January and 0.3 μg m<sup>-3</sup> in  
135 July.

Formatted: Font: (Default) Times New Roman

Formatted: Font: (Default) Times New Roman

136 However, none of the previous studies have systematically evaluated the  
137 changes in enhanced PM<sub>2.5</sub> concentrations through ARI and ACI in China at the  
138 long-term scale. Besides, the driving force and physical mechanisms for the  
139 changes are also yet to be explored. In this study, we try to investigate the  
140 enhanced PM<sub>2.5</sub> concentrations induced by ARI and ACI in 2013 over China, the  
141 impact of the changes in the meteorological background and anthropogenic  
142 emission from 2013 to 2021 on ARI- and ACI-induced PM<sub>2.5</sub> enhancements and  
143 its components. Furthermore, the causes of PM<sub>2.5</sub> enhancement changes are  
144 analyzed.

145

## 146 **2. Model and experimental design**

### 147 **2.1 Model configuration**

148 The Weather Research and Forecasting model with Chemistry (WRF-Chem)  
149 version 4.2 has been used in this study. The model domain covers the whole land  
150 area of China with a horizontal resolution of 27 km × 27 km. There are 24 vertical  
151 layers from surface to 50 hPa, with denser layers in the planetary boundary layer

152 (PBL). Major physical options used in the model include the Morrison double-  
153 moment scheme (Morrison et al., 2009), the Rapid Radiative Transfer Model for  
154 GCMs (RRTMG) shortwave and longwave radiative transfer schemes (Iacono et  
155 al., 2008), the Eta similarity surface-layer scheme (Janjic et al., 1994), the Noah  
156 land-surface model with multiple parameterization options (Niu et al., 2011), the  
157 Bougeault and Lacarrere PBL scheme (Bougeault et al., 1989), and the Grell-  
158 Freitas ensemble cumulus scheme (Grell et al., 2014). For chemistry, we employ  
159 the SAPRC-99 (Statewide Air Pollution Research Center mechanism, version  
160 1999) as the gas-phase chemistry mechanism (Carter et al., 2000). The aerosol  
161 module used in the study is the Model for Simulating Aerosol Interactions and  
162 Chemistry (MOSAIC) (Zaveri et al., 2008), which includes all major aerosol  
163 processes and represents the aerosol size distribution with 8 size bins. The  
164 MOSAIC also incorporates the one-dimensional Volatility Basis Set (VBS)  
165 framework that improves the simulation of secondary organic aerosol  
166 (Shrivastava et al., 2011). Rates for photolytic reactions are calculated using the  
167 Fast-J photolysis rate scheme (Wild et al., 2000). Additionally, we noted the poor  
168 ability of nitrate simulation in the WRF-Chem model. We improved the nitrate  
169 simulation by addressing the HONO underestimation in the model (Wang et al.,  
170 2015; Xue et al., 2020). More detailed information can be found in Section 1 in  
171 the Supplementary Information. The meteorological initial and boundary  
172 conditions are derived from the National Centers for Environmental Prediction  
173 Final Analysis reanalysis data with resolutions of  $1.0^\circ \times 1.0^\circ$  and 6 h

174 (<http://rda.ucar.edu/datasets/ds083.2/>). The chemical initial and boundary  
175 conditions are acquired from the simulation results of the National Center for  
176 Atmospheric Research's Community Atmosphere Model with Chemistry (CAM-  
177 Chem, before 2020, <https://www.acom.ucar.edu/cam-chem/cam-chem.shtml>) and  
178 the Whole Atmosphere Community Climate Model (WACCM, after 2020,  
179 <https://www.acom.ucar.edu/waccm/download.shtml>) with resolutions of  $0.94^\circ \times$   
180  $1.25^\circ$  and 6 h.

181 The anthropogenic emission data in China for 2013-2021 are obtained from  
182 the ABA-CAS-EI (Air Benefit and Cost and Attainment Assessment System-  
183 Emission Inventory) developed by Tsinghua University (Li et al., 2023). Specific  
184 emissions of SO<sub>2</sub>, NO<sub>x</sub> (NO and NO<sub>2</sub>), NH<sub>3</sub>, PM<sub>2.5</sub> and VOCs in 2013 and 2021  
185 are presented in Table S2. The emission data in other countries are obtained from  
186 the IIASA emission inventory for 2015 (Zheng et al., 2019; Gao et al., 2020). The  
187 biogenic emission is calculated online by the Model of Emissions of Gases and  
188 Aerosols from Nature (MEGAN) v2.04 (Guenther et al., 2006). The dust emission  
189 is calculated online by the Goddard Chemistry Aerosol Radiation and Transport  
190 (GOCART) model coupled with the MOSAIC aerosol schemes. (Zhao et al., 2010;  
191 2013)

192 To account for the physical processes of aerosol-radiation-cloud feedback  
193 on meteorological factors and PM<sub>2.5</sub>, the four-dimensional data assimilation  
194 (FDDA) is not utilized in our simulations. Aerosol optical depth, single scattering  
195 albedo, and asymmetry factors are calculated based on the Lorenz-Mie theory as



196 a function of wavelength and three-dimensional location (Fast et al., 2006). Then,  
197 the aerosol optical properties are transferred to the RRTMG radiation scheme to  
198 calculate the impact of aerosol on the radiation balance (Iacono et al., 2008). As  
199 for the ACI, activated aerosols are calculated by the Abdul-Razzak and Ghan  
200 scheme (Abdul-Razzak & Ghan, 2002) and are then coupled with the Morrison  
201 two-moment cloud microphysics scheme (Morrison et al., 2009). The prognostic  
202 cloud water content calculated by the Morrison scheme is input into the RRTMG  
203 scheme for the radiative transfer calculation. It should be noted that the prognostic  
204 aerosol does not influence cumulus clouds and ice nucleation in the model. The  
205 prognostic aerosol can only be activated as CCN. It does not directly contribute  
206 to ice nucleation, which is only influenced by air temperature and supersaturation  
207 (Kanji et al., 2017). Furthermore, CCN would influence grid-scale clouds.  
208 However, limited by the horizontal resolution of 27 km × 27 km, cumulus clouds  
209 could not be resolved in this grid.

210

## 211 **2.2 Experimental design**

212 As described in the introduction, the purpose of this study is to quantify the  
213 contributions of ARI and ACI to PM<sub>2.5</sub> concentrations under different emission  
214 scenarios. The simulation periods are January and July, 2013 and 2021,  
215 representing winter and summer, respectively.

216 As shown in Table 1, the enhanced PM<sub>2.5</sub> concentration induced by ARI and  
217 ACI could be obtained via comparing the simulation results with ARI or ACI

218 turned on or off. By setting the ‘aer\_ra\_feedback’ to 0 in the model, the ARI could  
 219 be turned off, which means that the interaction between aerosol and radiation is  
 220 prevented. The ACI could be turned off through prescribing the CDNC of  $25 \text{ cm}^{-3}$   
 221 in the microphysical scheme, which represents average level in the pristine air  
 222 (Bennartz et al., 2007). For example, the 13M13E\_B, 13M13E\_NR and  
 223 13M13E\_NRC shown in Table 1 represent the cases with ARI and ACI effects,  
 224 without ARI effect, and without ARI and ACI effects in 2013, respectively. The  
 225 ARI-induced  $\text{PM}_{2.5}$  enhancement could be acquired by comparing the results of  
 226 13M13E\_B and 13M13E\_NR; the ACI-induced  $\text{PM}_{2.5}$  enhancement could be  
 227 obtained by comparing the results of 13M13E\_NR and 13M13E\_NRC.

228

229 **Table 1. Case definition under different meteorological backgrounds and**  
 230 **anthropogenic emissions with ARI or ACI turned on or off.**

Case	Meteorology	Emission	ARI	ACI
13M13E_B	Jan & Jul, 2013	Jan & Jul, 2013	on	on
13M13E_NR	Jan & Jul, 2013	Jan & Jul, 2013	off	on
13M13E_NRC	Jan & Jul, 2013	Jan & Jul, 2013	off	off
21M13E_B	Jan & Jul, 2021	Jan & Jul, 2013	on	on
21M13E_NR	Jan & Jul, 2021	Jan & Jul, 2013	off	on
21M13E_NRC	Jan & Jul, 2021	Jan & Jul, 2013	off	off
21M21E_B	Jan & Jul, 2021	Jan & Jul, 2021	on	on
21M21E_NR	Jan & Jul, 2021	Jan & Jul, 2021	off	on

21M21E\_NRC    Jan & Jul, 2021    Jan & Jul, 2021    off    off

---

231

232        In order to obtain the changes of the ARI- and ACI-induced  $PM_{2.5}$   
233 enhancements from 2013 to 2021 caused by the variation of meteorological  
234 background and by the reduction of anthropogenic emission, the control  
235 experiments (21M13E; three experiments: with ARI and ACI turned on, with ARI  
236 turned off and ACI turned on, and with ARI and ACI turned off) are designed  
237 with the meteorological background in 2021 and the anthropogenic emission in  
238 2013. In the following, the 13M13E, 21M13E and 21M21E represent the cases  
239 with meteorological background and anthropogenic emission in 2013,  
240 meteorological background in 2021 and anthropogenic emission in 2013, and  
241 meteorological background and anthropogenic emission in 2021, respectively.  
242 Taking the ARI for example, the change of the ARI-induced  $PM_{2.5}$  enhancement  
243 from the variation of meteorological background is obtained by subtracting the  
244 ARI-induced  $PM_{2.5}$  enhancement in the 13M13E from that in the 21M13E [Eq.  
245 (1)]; the change in the ARI-induced  $PM_{2.5}$  enhancement from the reduction of  
246 anthropogenic emission is obtained by subtracting the ARI-induced  $PM_{2.5}$   
247 enhancement in the 21M13E from that in the 21M21E [Eq. (2)]. The calculations  
248 for the ACI-induced  $PM_{2.5}$  enhancement are similar, as shown in Eqs. (3) and (4).

249

$$ARI_{met} = (21M13E_B - 21M13E_{NR}) - (13M13E_B - 13M13E_{NR}), \quad (1)$$

$$ARI_{emi} = (21M21E\_B - 21M21E\_NR) - (21M13E\_B - 21M13E\_NR), \quad (2)$$

$$ACI_{met} = (21M13E\_NR - 21M13E\_NRC) - (13M13E\_NR - 13M13E\_NRC), \quad (3)$$

$$ACI_{emi} = (21M21E\_NR - 21M21E\_NRC) - (21M13E\_NR - 21M13E\_NRC), \quad (4)$$

250 where the  $ARI_{met}$  ( $ACI_{met}$ ) and  $ARI_{emi}$  ( $ACI_{emi}$ ) represent the changes of the  
 251 enhanced  $PM_{2.5}$  concentration induced by the ARI (ACI) from 2013 to 2021  
 252 caused by the variation of meteorological background and reduction of  
 253 anthropogenic emission, respectively.

254

### 255 **2.3 Model evaluation**

256 To determine the accuracy and reliability of simulation results, the  
 257 13M13E\_B and 21M21E\_B simulations (Table 1) are verified by using the  
 258 observations. The variables checked in the evaluation contain the concentration  
 259 and components of surface  $PM_{2.5}$  and the meteorological factors, including air  
 260 temperature (T2) and water vapor mixing ratio (Q2) at 2 m, wind speed (WS10)  
 261 and wind direction (WD10) at 10 m, as well as cloud fraction (CF) and liquid  
 262 water path (LWP).

263 Simulated temperature, wind, and water vapor are compared with the  
 264 observations from the National Climate Data Center (NCDC,  
 265 <http://www.ncdc.noaa.gov/>). The evaluation shows that the absolute errors for T2,

266 WS10 and Q2 are respectively less than 1°C, 1 m s<sup>-1</sup> and 0.1 g kg<sup>-1</sup> (Table S3),  
267 and those for WD10 are near or less than 10°. For the simulation utilizing the  
268 FDDA, the benchmarks of biases proposed by Emery et al. (2001) are 0.7°C, 0.6  
269 m s<sup>-1</sup>, 1.0 g kg<sup>-1</sup> and 20° for the T2, WS10, Q2 and WD10, respectively. The  
270 biases of the T2 and WS10 in our simulations have exceeded the benchmarks,  
271 while they are still similar to or smaller than in most previous WRF-Chem  
272 applications without FDDA over East Asia (Zhang et al., 2015; Zhao et al., 2017).

273 Simulated CF and LWP are compared with the data from the Moderate-  
274 resolution Imaging Spectroradiometer (MODIS) aboard the Terra satellite  
275 (<http://ladsweb.nascom.nasa.gov/data/search.html>). Overall, the CF and LWP  
276 simulations are in good agreement with the observations (Figs. S1 and S2). The  
277 high values of observed CF and LWP primarily appear in the south of China in  
278 January 2013 and 2021, and high value of CF also occurs in the NCP region. The  
279 high values of CF and LWP in the south of China could be reproduced in the  
280 simulation, while the CF in NCP region is slightly underestimated, which could  
281 be owing to imperfect cloud parameterization scheme in the model or  
282 uncertainties in the retrieval of MODIS datasets. In July 2013 and 2021, part of  
283 high value area of observed LWP and most high value area of observed CF appear  
284 in the southwestern China and the east coast of China, which also could be  
285 captured by the simulation. In addition, high LWP also appears in Gansu and  
286 Sichuan Provinces in July 2013 and in the YRD and Sichuan-Chongqing in July  
287 2021, which are both well reproduced. The distributions of low values of

Deleted: 1

289 observed CF and LWP in January and July of 2013 and 2021 are also well  
290 simulated.

291 The simulation of surface PM<sub>2.5</sub> concentration is compared with the data  
292 from the China National Environmental Monitoring Center  
293 (<https://quotsoft.net/air/>). The evaluation shows that both the regional average  
294 value and spatial distribution of simulated PM<sub>2.5</sub> concentration are in good  
295 agreement with the observational data. As shown in Fig. S3, the biases of regional  
296 average PM<sub>2.5</sub> concentration in January and July of 2013 and 2021 are below 3  
297 μg m<sup>-3</sup> in eastern China. In this study, the eastern China includes most of Chinese  
298 provinces except Xinjiang, Xizang, Ningxia, Qinghai, Gansu, Inner-Mongolia  
299 and Heilongjiang Provinces, which contains most polluted regions in China. In  
300 addition, the distributions of high simulated PM<sub>2.5</sub> concentration are also  
301 consistent with the observations, such as the NCP region, the YRD region, and  
302 the Sichuan-Chongqing area.

303 The simulated PM<sub>2.5</sub> components are also reasonable compared with the  
304 observation data. Given that the PM<sub>2.5</sub> components data in 2013 are very rare, we  
305 sourced three sets of data in January 2013, respectively in Beijing (Mattias et al.,  
306 2017), Handan (Zhang et al., 2015), and Shanghai (Li et al., 2015). The results  
307 show that the simulated PM<sub>2.5</sub> components are reproduced well generally.  
308 Specifically, the simulated PM<sub>2.5</sub> components are larger than half of observational  
309 PM<sub>2.5</sub> components and less than the double observational PM<sub>2.5</sub> components (Fig.  
310 S4). Observed PM<sub>2.5</sub> components data in 2021 are, from a data sharing platform

Deleted: T

Deleted: , which

Deleted: is

Formatted: Subscript

314 for the NCP region and its surrounding areas (Wang et al., 2019). Fig. S5 shows  
315 the ratios of observation to simulation of ammonium, sulfate, BC and organic  
316 carbon (OC) in January and July 2021. The results exhibit that almost all the ratios  
317 of PM<sub>2.5</sub> components are located between 0.5 and 2.0, while some ratios of sulfate  
318 in January, part of OC in January, and BC in January and July are beyond this  
319 range. But these discrepancies will not cause obvious uncertainties in this  
320 research. Specifically, considering BC low hygroscopicity, BC overestimations  
321 in January and July 2021 probably bring low uncertainties in ACI-induced PM<sub>2.5</sub>  
322 enhancement. To test the impact of simulated BC overestimation in January 2021  
323 on ARI-induced PM<sub>2.5</sub> enhancement, we utilize another set of particulate matter  
324 (PM) source profiles (Liu et al., 2018) and conduct the simulations for January  
325 2021. The results indicate that the ratios of simulated BC concentration to  
326 observational BC concentration are within 2.0. The ARI-induced PM<sub>2.5</sub>  
327 enhancement is 1.33  $\mu\text{g m}^{-3}$ , which shows a negligible difference from the result  
328 (1.37  $\mu\text{g m}^{-3}$ ) obtained using original PM source profiles (Fig. S6). In view of the  
329 results in January 2021, the BC overestimation in July 2021 also probably brings  
330 low uncertainties in ARI-induced PM<sub>2.5</sub> enhancement. However, the reduction in  
331 simulated BC concentration in January 2021 does not necessarily mean that this  
332 set of PM source profiles is better than the original PM source profiles, because  
333 this might be an accidental result caused by other uncertainties. For example, the  
334 current model underestimates the wet deposition of BC due to neglecting the  
335 increase in BC hygroscopicity brought about by BC aging. If this process is

336 considered in the model, simulated BC concentrations might be better reproduced  
337 using original PM source profiles. Therefore, in this study, we still use the original  
338 results for our analysis. The model also underestimates the sulfate concentration  
339 and overestimates the part of OC concentration in January 2021. We think that  
340 neither of these discrepancies will cause significant uncertainties in ARI- and  
341 ACI-induced PM<sub>2.5</sub> enhancement. Specifically, the majority of aerosol is  
342 scattering aerosol and the PM<sub>2.5</sub> concentration in January 2021 is reproduced well.  
343 Therefore, we think that the impact of the sulfate underestimation on the ARI-  
344 induced PM<sub>2.5</sub> enhancement would be largely offset by the overestimation of  
345 other scattering aerosol components, such as OC. In addition, the OC  
346 overestimation should not bring significant uncertainty to ACI-induced PM<sub>2.5</sub>  
347 enhancement either, because of the relatively lower hygroscopicity of OC  
348 compared to secondary inorganic aerosol. The underestimation of sulfate  
349 simulation in January 2021 also minimally affects ACI-induced PM<sub>2.5</sub>  
350 enhancement because the sulfate underestimation mainly occurs in the North  
351 China Plain, where cloud cover is low. In contrast, in southern cities such as  
352 Mianyang city in Sichuan province where there is plenty of cloud cover, the  
353 sulfate simulation was 4.19  $\mu\text{g m}^{-3}$  in January 2021, which is very close to the  
354 observed value of 4.25  $\mu\text{g m}^{-3}$  (Lin et al., 2022).

355 In summary, the performances of WRF-Chem model on the simulations of  
356 air quality and meteorological factors over China are fairly good, and the  
357 differences between simulations and observations are reasonable and acceptable.

**Deleted:** Fig. S4 shows the ratios of observation to simulation of ammonium, nitrate, sulfate, BC and organic carbon (OC) in January and July 2021. The results exhibit that almost all the ratios of PM<sub>2.5</sub> components are located between 0.5 and 2.0, while some ratios of sulfate in January and BC in January and July are beyond this range, but not far away. Such minor discrepancies will not cause obvious uncertainty in this research.



366

### 367 **3. Results and discussion**

#### 368 **3.1 The impacts of ARI and ACI feedbacks on the meteorological** 369 **factors and PM<sub>2.5</sub> concentrations in 2013**

370 We comprehensively discuss the effects of ARI and ACI on the regional  
371 meteorological factors and PM<sub>2.5</sub> concentrations in January and July 2013. Fig. 1  
372 shows the impacts of ARI and ACI feedbacks on the SWDOWN, PBLH, T2, RH  
373 and PM<sub>2.5</sub> concentration in January and July 2013. For the ARI, the SWDOWN  
374 decreases by ~~18.37~~ and ~~7.71~~ W m<sup>-2</sup> in January and July 2013 in eastern China,  
375 respectively. Since the incoming solar radiation reaching the ground is reduced  
376 by PM, the T2 and PBLH in eastern China further decrease by 0.30 and 0.03°C,  
377 and 28.34 and 8.75 m in January and July 2013, respectively. Meanwhile, the RH  
378 increases by 0.46% and 0.08% due to the water vapor accumulation in the  
379 suppressed planetary boundary layer (Liu et al., 2018). Ultimately, the PM<sub>2.5</sub>  
380 concentration increases by 5.59 and 0.13 μg m<sup>-3</sup> in eastern China (Fig. 1d). For  
381 the ACI, affected by the cloud modified by the aerosol, the SWDOWN, T2 and  
382 PBLH decrease by 7.54 and 14.03 W m<sup>-2</sup>, 0.18 and 0.17 °C, and 10.89 and 24.31  
383 m, and the RH increases by 0.34% and 0.37% in January and July 2013 in eastern  
384 China, respectively. As a result, the PM<sub>2.5</sub> concentration increases by 3.96 and  
385 2.20 μg m<sup>-3</sup> in eastern China. Fig. 2 shows that the regional averaged values and  
386 spatial distributions of PM<sub>2.5</sub> enhancements induced by ARI and ACI in 2013 are  
387 in line with the results of previous studies (Zhao et al., 2017; Zhang et al., 2018).

Deleted: 26

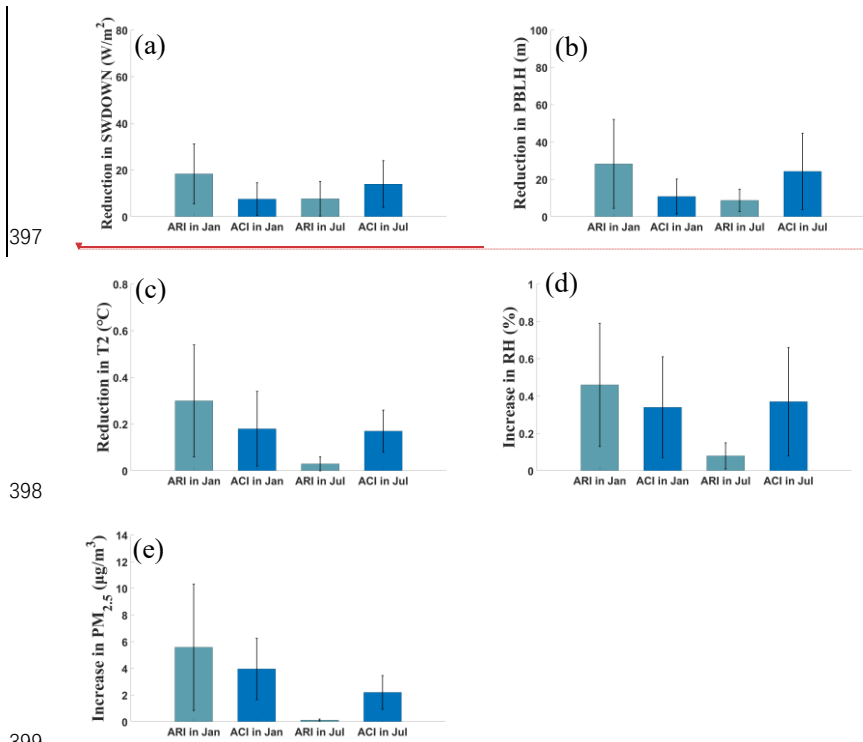
Deleted: 55

Deleted: 15

Deleted: 28

392 Overall, the enhanced  $PM_{2.5}$  concentration induced by ARI is greater than  
 393 that induced by ACI in January 2013, which is due to the relatively low LWP in  
 394 the high  $PM_{2.5}$  concentration area. But it shows the opposite situation in July 2013,  
 395 owing to the plentiful cloud in warm July (Zhang et al., 2018).

396



397

398

399

400 Fig. 1. The regional averaged reductions of (a) downward shortwave radiation at  
 401 the surface (SWDOWN), (b) planetary boundary layer height (PBLH), (c) 2-m  
 402 air temperature (T2), and increments of (d) relative humidity (RH) and (e) fine  
 403 particulate matter ( $PM_{2.5}$ ) concentration induced by the aerosol-radiative  
 404 interaction (ARI) and aerosol-cloud interaction (ACI) in January and July 2013

Deleted: er

Deleted:

407 in eastern China, the error bars represent the standard deviations for different  
408 meteorological factors and PM<sub>2.5</sub> concentration induced by ARI and ACI in  
409 January and July 2013 in eastern China.

410

### 411 **3.2 The shift of the PM<sub>2.5</sub> enhancements induced by ARI and ACI**

412 As discussed in section 3.1, the enhanced PM<sub>2.5</sub> concentrations induced by  
413 ARI and ACI exhibit obvious spatial and seasonal variations in 2013. However,  
414 due to the variations of meteorological background and the reduction of  
415 anthropogenic emission from 2013 to 2021, their joint and individual impacts on  
416 the ARI- and ACI-induced PM<sub>2.5</sub> enhancements are still unclear. Fig. 2 shows the  
417 ARI- and ACI-induced PM<sub>2.5</sub> enhancements in the experiments of 13M13E,  
418 21M13E and 21M21E in January and July.

419 As shown in Fig. 2, from 2013 to 2021, the PM<sub>2.5</sub> concentration  
420 enhancement induced by the ARI in January decreases by 75% (from 5.59 to 1.37  
421  $\mu\text{g m}^{-3}$ ). Zhang et al. (2022) also found that the ARI effect over China weakens  
422 during 2013–2017, and the ratio of PM<sub>2.5</sub> enhancement to the ambient PM<sub>2.5</sub>  
423 concentration decreases from 5.40% to 3.30%. The decline of the PM<sub>2.5</sub>  
424 enhancement ratio (2.10%) is lower than that in this study (3.26%) due to the  
425 continuous emission reduction after 2017. On the other hand, the ACI-induced  
426 PM<sub>2.5</sub> enhancement decreases by 51%, from 3.96 to 1.93  $\mu\text{g m}^{-3}$ . With lower  
427 percentage decrease in the PM<sub>2.5</sub> enhancement, the ACI-induced PM<sub>2.5</sub>  
428 enhancement exceeds the ARI-induced PM<sub>2.5</sub> enhancement in January 2021. In

429 July, both the ARI- and ACI-induced PM<sub>2.5</sub> enhancements show decreasing trends,  
430 the percentage decreases of the ARI-induced (31%) and ACI-induced (34%)  
431 PM<sub>2.5</sub> enhancements are very close.

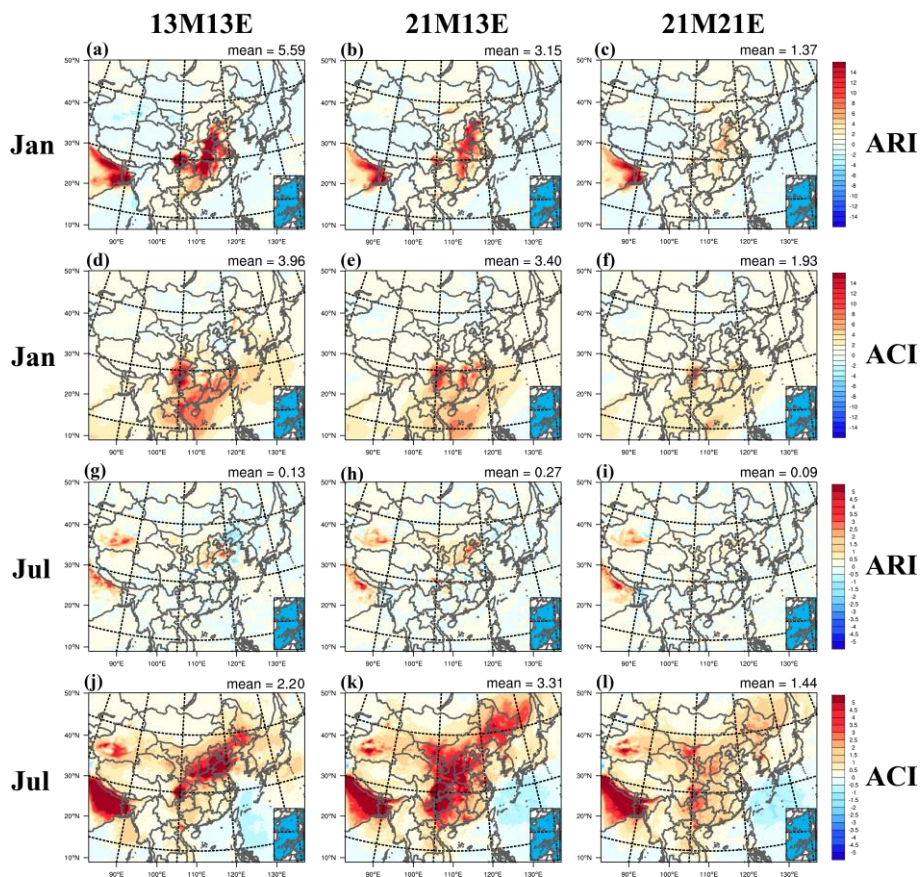
432 The contributions of the meteorological background variation and  
433 anthropogenic emission reduction to the changes of the ARI- and ACI-induced  
434 PM<sub>2.5</sub> enhancements are different. Due to the meteorological background change  
435 from 2013 to 2021, the ARI- and ACI-induced PM<sub>2.5</sub> enhancements show  
436 different characteristics in January and July. It can be seen that, the ARI-induced  
437 PM<sub>2.5</sub> enhancement decreases from 5.59 to 3.15  $\mu\text{g m}^{-3}$  with the variation of  
438 meteorological background in January, while it increases from 0.13 to 0.27  $\mu\text{g m}$   
439  $^{-3}$  in July. The primary reason for the difference is that the ambient PM<sub>2.5</sub>  
440 concentration decreases in January but increases in July caused by different  
441 meteorological backgrounds. The ACI-induced PM<sub>2.5</sub> enhancement changes  
442 slightly from 3.96 to 3.40  $\mu\text{g m}^{-3}$  in January due to the variation of meteorological  
443 background. However, it increases from 2.20 to 3.31  $\mu\text{g m}^{-3}$  in July, because of  
444 a large aerosol-induced LWP increase in July 2021.

445 Considering the reduction of anthropogenic emission, the ARI- and ACI-  
446 induced PM<sub>2.5</sub> enhancements both show declining trends (middle and right  
447 columns in Fig. 2). The ARI-induced PM<sub>2.5</sub> enhancement decreases by 56.51% in  
448 January, from 3.15 to 1.37  $\mu\text{g m}^{-3}$ . The ACI-induced PM<sub>2.5</sub> enhancement  
449 decreases by 43.24%, from 3.40 to 1.93  $\mu\text{g m}^{-3}$ . The percentage decrease of the  
450 ACI-induced PM<sub>2.5</sub> enhancement is lower than that of the ARI-induced in January,

451 which also occurs in July, when the ARI-induced  $PM_{2.5}$  enhancement decreases  
452 by 66.67% (from 0.27 to 0.09  $\mu\text{g m}^{-3}$ ) and ACI-induced  $PM_{2.5}$  enhancement  
453 decreases by 56.50% (from 3.31 to 1.44  $\mu\text{g m}^{-3}$ ).

454 In summary, both the variation of meteorological background and the  
455 reduction of anthropogenic emission play important roles in changing the ARI-  
456 and ACI-induced  $PM_{2.5}$  enhancements. However, the decreases of ARI- and ACI-  
457 induced  $PM_{2.5}$  enhancements from 2013 to 2021 are primarily attributed to the  
458 reduction of anthropogenic emission. In addition, the percentage decrease of the  
459 ACI-induced  $PM_{2.5}$  enhancement is lower than that induced by the ARI in both  
460 January and July. Therefore, the ACI-induced  $PM_{2.5}$  enhancement has become  
461 increasingly important in both January and July from 2013 to 2021.

462



463  
 464 Fig. 2. The distributions of enhanced PM<sub>2.5</sub> concentrations (unit:  $\mu\text{g m}^{-3}$ ) induced  
 465 by the ARI (first and third rows) and the ACI (second and fourth rows) in January  
 466 (first and second rows) and July (third and fourth rows) in the experiments of  
 467 13M13E (left column), 21M13E (middle column) and 21M21E (right column).

468  
 469 **3.3 The changes in the enhanced PM<sub>2.5</sub> components induced by the**  
 470 **ARI and the ACI**

471 In terms of the anthropogenic emission reduction, the percentage decrease

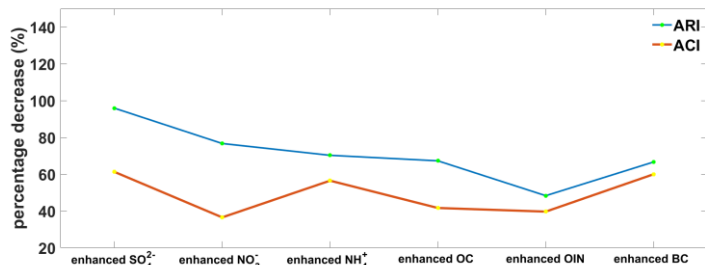
472 of the ACI-induced PM<sub>2.5</sub> enhancement is lower than that induced by the ARI in  
473 both January and July. We find that the difference is primarily from the different  
474 percentage decreases of the secondary PM<sub>2.5</sub> component enhancements induced  
475 by ARI and ACI.

476 Fig. 3 shows the percentage decreases of ARI- and ACI-induced PM<sub>2.5</sub>  
477 component enhancements caused by the anthropogenic emission reduction in  
478 January and July. It can be seen that the difference between the percentage  
479 decreases of the ARI- and ACI-induced enhancements of sulfate, nitrate,  
480 ammonium and OC is larger than those of BC and other inorganic aerosol (OIN),  
481 OIN refers to inorganic compositions other than sulfate, nitrate, ammonium, and  
482 BC. These compositions include sea salt and mineral elements. Specifically, the  
483 difference between the percentage decreases for sulfate, nitrate, ammonium and  
484 OC enhancements are 34.66%, 40.20%, 13.80% and 25.65% respectively, and the  
485 values for OIN and BC are 8.67% and 6.67%. This result indicates that the lower  
486 decrease in the ACI-induced PM<sub>2.5</sub> concentration enhancement is mainly due to  
487 the small decrease in the ACI-induced enhancements of secondary PM<sub>2.5</sub>  
488 components. The main causes will be illustrated in section 3.4.

489

Deleted: and BC

Deleted:



492  
493 Fig. 3. Percentage decreases (21M13E–21M21E)/21M13E) of the spatial and  
494 temporal average ARI- and ACI-induced PM<sub>2.5</sub> component enhancements in  
495 eastern China in January and July caused by the anthropogenic emission  
496 reduction from 2013 to 2021.

Deleted: Fig. 3. The percentage decreases (21M13E–21M21E)/21M13E) of the ARI- and ACI-induced PM<sub>2.5</sub> component enhancements caused by the reduction of anthropogenic emission from 2013 to 2021.

### 498 3.4 Causes for the increased importance of ACI

#### 499 3.4.1 Explanation from the perspective of meteorological changes

500 As discussed in previous studies, the decrease of PBLH and T2 and the  
501 increase of RH are tightly related to the ARI- and ACI-induced PM<sub>2.5</sub>  
502 enhancements (Donahue et al., 2012; Ding et al., 2016; Moch et al., 2022; Liu et  
503 al., 2018). From the perspective of the ARI- and ACI-induced changes in  
504 meteorological factors, we investigate the primary reasons for the increasing  
505 importance of the ACI-induced PM<sub>2.5</sub> enhancement under the reduction of  
506 anthropogenic emission.

507 Fig. 4 shows the percentage decreases of ARI- and ACI-induced decrease of  
508 SWDOWN, PBLH and T2 and increase of RH due to the reduction of  
509 anthropogenic emission from 2013 to 2021. In January, in order to illustrate the



514 reasons of the lower percentage decrease in the ACI-induced  $PM_{2.5}$  enhancement  
515 clearly, we take the highly polluted NCP region as an example. As shown in Fig.  
516 4c, the percentage decreases of the ACI-induced decline of SWDOWN (19%),  
517 PBLH (27%) and T2 (20%) and the increase of RH (24%) are lower than those  
518 of the ARI-induced decline of SWDOWN (29%), PBLH (39%) and T2 (32%) and  
519 the increase of RH (36%). The phenomenon in July is similar with that in January  
520 (Figs. 4a and b). To our knowledge, the PBLH and T2 are determined by the  
521 incoming solar radiation at the surface, and they can strongly influence the RH.  
522 So the lower percentage decrease in the ACI-induced reductions of PBLH and T2  
523 and increase of RH could be explained by the lower percentage decrease in the  
524 ACI-induced SWDOWN reduction.

525 We believe that the relatively lower decrease in the ACI-induced SWDOWN  
526 reduction is inevitable under high ambient  $PM_{2.5}$  concentration. As shown in Fig.  
527 S8b, the SWDOWN reduction induced by the ARI shows a linear relationship  
528 with the decline of ambient  $PM_{2.5}$  concentration, which is similar with Zhou et al.  
529 (2018). In contrast, the decrease in the SWDOWN reduction induced by the ACI  
530 is lower than that by the ARI due to the ambient  $PM_{2.5}$  decrease in the high  $PM_{2.5}$ -  
531 polluted regime. The reason is that the decrease in ambient  $PM_{2.5}$  concentration  
532 directly weakens the ARI-induced SWDOWN reduction, but it has only a minor  
533 impact on the ACI-induced SWDOWN reduction because the change in LWP and  
534 cloud effective radius ( $Re$ ) induced by ACI is not sensitive to  $PM_{2.5}$  reduction in  
535 the  $PM_{2.5}$ -polluted regime. In our simulations, the influence of ACI-induced  $Re$

Deleted: 5

537 change is relatively smaller than that of ACI-induced LWP change with a large  
538 decrease in PM<sub>2.5</sub> concentration (Fig. S7). Therefore, we are only concerned with  
539 change in ACI-induced LWP with a reduction in PM<sub>2.5</sub>. As shown in Fig. S8, when  
540 the ambient PM<sub>2.5</sub> concentration exceeded 15 μg m<sup>-3</sup>, the decrease in ACI-  
541 induced LWP increase is relatively low with a PM<sub>2.5</sub> reduction from 120 to 15 μg  
542 m<sup>-3</sup>, indicating that aerosols are not a key limiting factor to cloud formation in  
543 this range. Note that when the ambient PM<sub>2.5</sub> concentration decreases to 15, μg  
544 m<sup>-3</sup>, the weakening of SWDOWN reduction induced by the ACI might be larger  
545 than that by the ARI. This is because decrease in ACI-induced LWP increase is  
546 relatively fast, with a PM<sub>2.5</sub> reduction from 15 to 0 μg m<sup>-3</sup>. Previous studies have  
547 demonstrated that the decrease in ACI-induced LWP increase is relatively fast or  
548 slow with the ambient PM<sub>2.5</sub> reduction in the PM<sub>2.5</sub>-clean or polluted condition,  
549 respectively (Myhre et al., 2007; Savane et al., 2015). The regional and temporal  
550 average PM<sub>2.5</sub> concentration in eastern China in January and July simulated using  
551 background meteorology in 2021 and emissions in 2013 is 63 and 25 μg m<sup>-3</sup>,  
552 which is much higher than 15 μg m<sup>-3</sup>. Therefore, the decrease in ACI-induced  
553 SWDOWN reduction in both months is weak,

554 Especially, the lower PBLH caused by ARI and ACI will enhance the  
555 accumulation of all the PM<sub>2.5</sub> components, but higher RH and lower T2 induced  
556 by the ARI and ACI could promote the production of extra secondary PM<sub>2.5</sub>  
557 components through strengthening aqueous and heterogeneous reactions and  
558 causing gas precursors to condense into particle matter (Donahue et al., 2012; Liu

**Deleted:** The reason is that the decrease in the ambient PM<sub>2.5</sub> concentration directly weakens the ARI-induced SWDOWN reduction, but it has minor impact on the ACI-induced LWP and cloud effective radius (Re) because high ambient PM<sub>2.5</sub> concentration still provides enough CCN (Gryspeerd et al., 2019; Yang et al., 2019; Liu et al., 2020).

**Deleted:** 20

**Formatted:** Font: (Default) Times New Roman

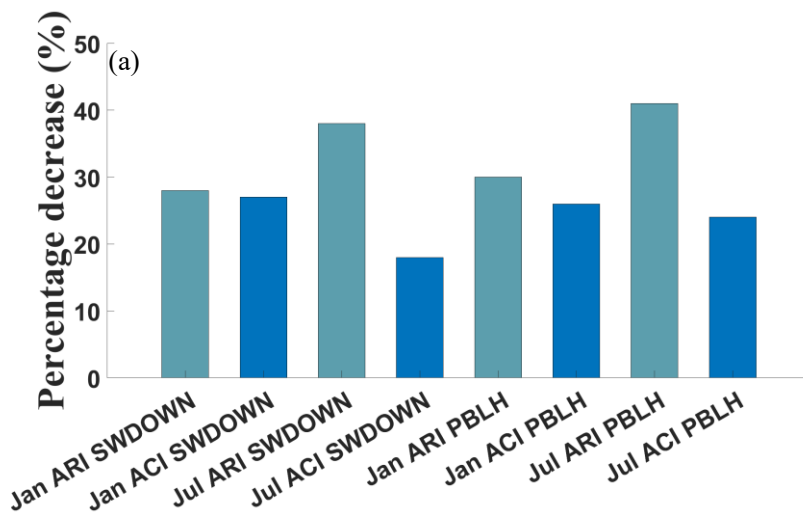
**Formatted:** Font: (Default) Times New Roman

**Formatted:** Font: (Default) Times New Roman

**Deleted:** , because the decrease in ambient PM<sub>2.5</sub> concentration will reduce the CCN under the PM<sub>2.5</sub>-clean condition, which will reduce CF, cloud water content and increase Re (Yang et al., 2019; Liu et al., 2020).

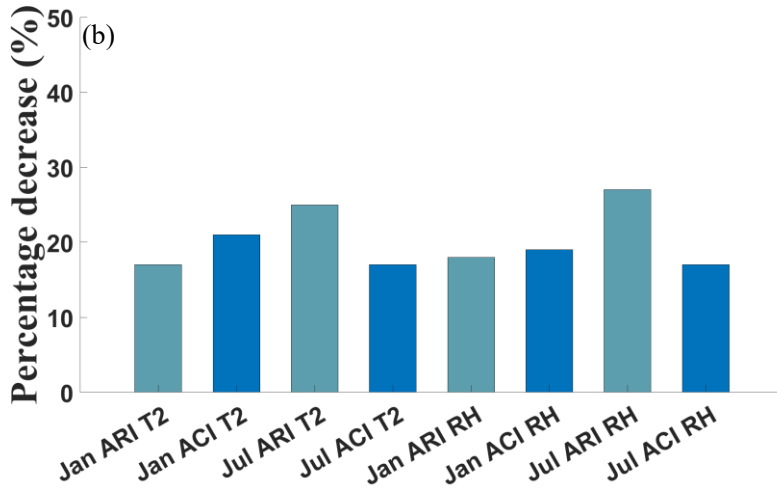
570 et al., 2018). Therefore, lower percentage decrease in the T2 reduction and RH  
571 increase induced by the ACI is more likely to weaken the decrease in the  
572 enhancements of secondary PM<sub>2.5</sub> components. This well explains the lower  
573 percentage decreases in the enhancements of secondary PM<sub>2.5</sub> components  
574 induced by the ACI than those by the ARI as shown in Fig. 3.

575



576

577



578



579

580 Fig. 4. The percentage decreases of the regional averages of (a) the decrease of  
 581 SWDOWN and PBLH, and (b) the T2 reduction and RH increase induced by ARI  
 582 and ACI in eastern China caused by the anthropogenic emission reduction in  
 583 January and July from 2013 to 2021. (c) is the same as (a) and (b), but in the NCP  
 584 region in January.

585

### 586 3.4.2 Explanation from the perspective of PM<sub>2.5</sub> concentration distribution 587 changes

588 Ambient PM<sub>2.5</sub> concentration is the fundamental factor to trigger the ARI  
589 and the ACI. In order to further explore the reasons for the increasing importance  
590 of enhanced PM<sub>2.5</sub> concentration induced by ACI, we discuss the characteristics  
591 of enhanced PM<sub>2.5</sub> concentration induced by ARI and ACI under different PM<sub>2.5</sub>  
592 pollution levels. Given that this study mainly focuses on the change in ARI- and

593 ACI-induced PM<sub>2.5</sub> enhancement in the PM<sub>2.5</sub>-polluted regime, we only discuss  
594 these changes within the PM<sub>2.5</sub> concentration range of 15–180 μg m<sup>-3</sup>

595 The PM<sub>2.5</sub> concentration is divided into 11 levels from 15 to 180 μg m<sup>-3</sup>. As  
596 shown in Fig. 5a, in the heavily PM<sub>2.5</sub>-polluted regime (135–180 μg m<sup>-3</sup>), the  
597 decrease in SWDOWN induced by ARI is much larger than that induced by ACI  
598 (Fig. S9a). Then, the decrease in PBLH and T2 and the increase in RH induced  
599 by ARI are also larger than those induced by ACI (Fig. S9b–d). Thus, the  
600 enhanced PM<sub>2.5</sub> induced by the ARI is much larger than that by the ACI (Fig. 5a).  
601 However, when the PM<sub>2.5</sub> concentration decrease to the range of 15–45 μg m<sup>-3</sup>,  
602 the decrease in SWDOWN, PBLH, and T2 and the increase in RH induced by  
603 ACI significantly exceed those induced by ARI. Thus, the ACI-induced PM<sub>2.5</sub>  
604 enhancement significantly exceeds the ARI-induced PM<sub>2.5</sub> enhancement and  
605 becomes more important. This indicates the fast decrease in the ARI-induced  
606 PM<sub>2.5</sub> enhancement and the increasing contribution of the ACI-induced PM<sub>2.5</sub>

Formatted: Subscript

Formatted: Subscript

Formatted: Subscript

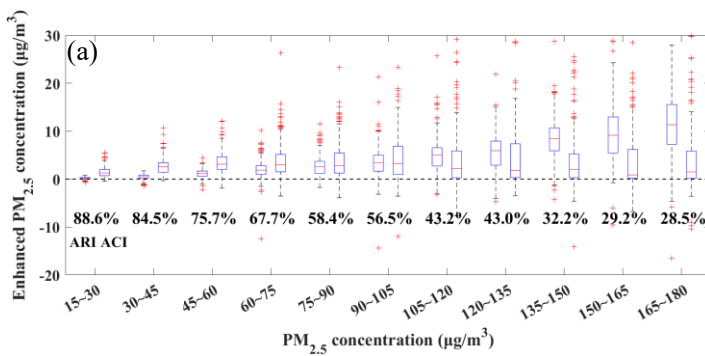
Deleted: 2

Deleted: 0

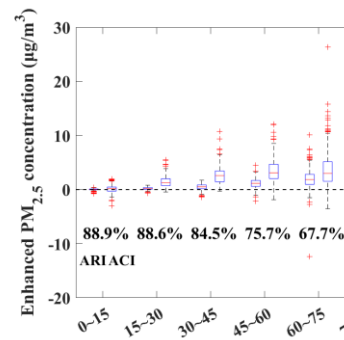
Deleted: As shown in Fig. 5a, under the heavy PM<sub>2.5</sub>-polluted regime (135–180 μg m<sup>-3</sup>), the enhanced PM<sub>2.5</sub> induced by the ARI is much larger than that by the ACI, while the ACI-induced PM<sub>2.5</sub> enhancement will obviously exceed the ARI-induced PM<sub>2.5</sub> enhancement in the PM<sub>2.5</sub>-clean condition (0–45 μg m<sup>-3</sup>). It indicates the fast decrease in the ARI-induced PM<sub>2.5</sub> enhancement and the increasing contribution of the ACI-induced enhancement with the decrease of PM<sub>2.5</sub> concentration. As illustrated in section 3.4.1, the lower percentage decrease in the ACI-induced PM<sub>2.5</sub> enhancement with the decrease of PM<sub>2.5</sub> concentration is because of the lower percentage decrease in the ACI-induced SWDOWN reduction, which is due to the lower decrease in the LWP caused by the ambient PM<sub>2.5</sub> decrease in the heavy PM<sub>2.5</sub>-polluted regime.

624 enhancement with the decrease in the  $PM_{2.5}$  concentration. In summary, the  
 625 percentage decrease in the  $PM_{2.5}$  enhancement induced by ACI is weaker than  
 626 that induced by ARI with the decrease of  $PM_{2.5}$  concentration because of the  
 627 lower percentage decrease in the ACI-induced SWDOWN, which causes the  
 628 lower percentage decrease in the ACI-induced PBLH and T2 reduction and the  
 629 RH increase. Furthermore, as shown in Fig. S8a, the low percentage decrease in  
 630 the ACI-induced SWDOWN reduction is due to a low decrease in the ACI-  
 631 induced LWP in the  $PM_{2.5}$ -polluted regime. Considering the decrease in the  
 632 ambient  $PM_{2.5}$  concentration due to the anthropogenic emission reduction from  
 633 2013 to 2021 (Fig. 5b), the ACI-induced  $PM_{2.5}$  enhancement certainly contributes  
 634 more to the total  $PM_{2.5}$  concentration in 2021.

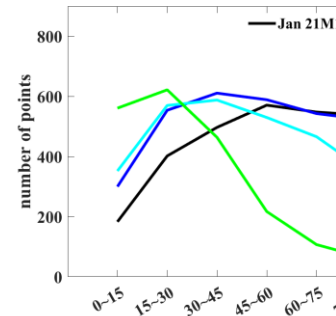
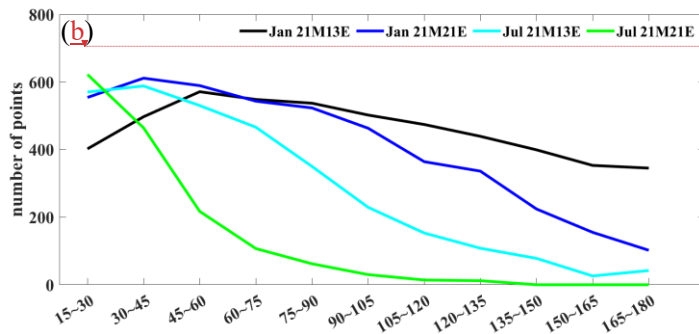
635



636



Deleted:



Deleted:

Deleted: a

Deleted: Fig. 5. (a) The enhanced  $PM_{2.5}$  concentrations induced by ARI and ACI under different ambient  $PM_{2.5}$  levels. The percentage represents the ratio of the ACI-induced  $PM_{2.5}$  enhancement to the sum of ARI- and ACI-induced  $PM_{2.5}$  enhancements. (b) The distributions of ambient  $PM_{2.5}$  levels in January and July in the experiments of 21M13E and 21M21E.

638  
639  
640  
641  
642  
643  
644  
645  
646

Fig. 5. (a) The enhanced  $PM_{2.5}$  concentrations induced by ARI and ACI at different ambient  $PM_{2.5}$  levels. These data are from the simulations for January and July in the experiments of 21M13E and 21M21E. The percentage represents the ratio of the ACI-induced  $PM_{2.5}$  enhancement to the sum of ARI- and ACI-induced  $PM_{2.5}$  enhancements. (b) The distributions of ambient  $PM_{2.5}$  levels in January and July in the experiments of 21M13E and 21M21E.

#### 4. Conclusions

Under the background of sharped anthropogenic emission reduction, this study investigates changes of the ARI- and ACI-induced  $PM_{2.5}$  enhancements for 2013–2021, and explores the causes for these changes from the perspectives of meteorological factors and  $PM_{2.5}$  concentration distribution.

The results show that the enhanced  $PM_{2.5}$  induced by the ARI ( $5.59 \mu g m^{-3}$ ) is greater than that by the ACI ( $3.96 \mu g m^{-3}$ ) in January 2013. However, the ARI- and ACI-induced  $PM_{2.5}$  enhancements decrease from  $5.59$  and  $3.96 \mu g m^{-3}$  to  $1.37$  and  $1.93 \mu g m^{-3}$  in January and decrease by 75% and 51% for 2013–2021. The

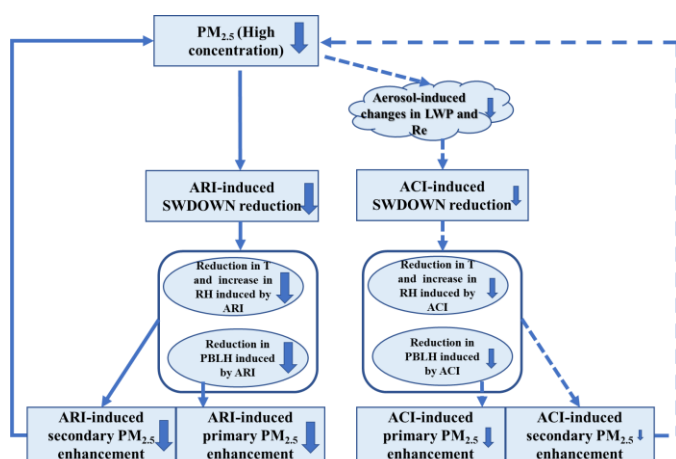
663 smaller decrease ratio (51%) for ACI-induced  $PM_{2.5}$  enhancements implies that  
664 ACI becomes more important for enhancing  $PM_{2.5}$  concentrations in January  
665 2021. Furthermore, we separated the contributions of meteorological background  
666 variation and anthropogenic emission reduction. Compared with the  
667 meteorological background variation, anthropogenic emission reduction plays a  
668 more important role in causing the decrease of ARI- and ACI-induced  $PM_{2.5}$   
669 enhancements. Owing to only emission reduction, the enhanced  $PM_{2.5}$   
670 concentrations induced by the ARI and ACI decrease by 56% and 43% in January  
671 and 66% and 56% in July, respectively. The ACI-induced  $PM_{2.5}$  enhancement  
672 becomes increasingly important in both January and July for 2013–2021. More  
673 specifically, the lower percentage decrease in the ACI-induced  $PM_{2.5}$   
674 enhancement is dominated by the lower decrease in the enhancements of  
675 secondary  $PM_{2.5}$  components.

676 The lower percentage decrease in the enhanced  $PM_{2.5}$  induced by the ACI is  
677 due to the lower percentage decrease in the ACI-induced SWDOWN reduction,  
678 which is because of the lower decrease in the LWP and increase in the  $Re$  caused  
679 by the ambient  $PM_{2.5}$  decrease in the high  $PM_{2.5}$ -polluted regime (Fig. 6). At the  
680 same time, the lower percentage decreases in the T2 reduction and RH increase  
681 induced by the ACI further lead to the lower percentage decrease in the  
682 enhancements of the ACI-induced secondary  $PM_{2.5}$  components (Fig. 6). Notably,  
683 due to relative lower percentage decrease in the ACI-induced SWDOWN  
684 reduction in the high  $PM_{2.5}$ -polluted regime, the increasing importance of ACI-



685 induced  $PM_{2.5}$  enhancement is a matter of course with the ambient  $PM_{2.5}$  decrease.

686



687

688 Fig. 6. Schematic diagram for the decrease of ARI- and ACI-induced primary and  
689 secondary  $PM_{2.5}$  enhancement due to reduction in ambient  $PM_{2.5}$  concentration.

690 Solid arrows represent these processes are strongly weakened; dotted arrows  
691 represent these processes are slightly weakened.

692

693 This study has important implication for the  $PM_{2.5}$  control. As we know,  
694 ARI- and ACI-induced  $PM_{2.5}$  enhancements have a non-negligible contribution  
695 to the deterioration of  $PM_{2.5}$  air quality. Previous research has investigated the  
696 impact of anthropogenic emission reduction on the ARI-induced  $PM_{2.5}$   
697 enhancement (Zhou et al., 2019). But compared with  $PM_{2.5}$  enhancement induced  
698 by ARI, that induced by ACI is more complicated and harder to be alleviated. Our  
699 findings have further revealed that the ACI-induced  $PM_{2.5}$  enhancement is getting  
700 more important relative to that induced by ARI. This is especially true in cloud-

Formatted: Justified, Indent: First line: 0 ch

701 prone areas like Sichuan-Chongqing area, which have witnessed rather weak  
702 decreases of ACI-induced  $PM_{2.5}$  concentration in the past decade due to weak  
703 decreases of aerosol-induced LWP under the condition of high ambient  $PM_{2.5}$   
704 level (Fig. 2). The ACI-induced  $PM_{2.5}$  enhancement needs to be considered more  
705 seriously in the formulation of control polices to meet national  $PM_{2.5}$  air  
706 quality standard, especially in cloud-prone areas with high ambient  $PM_{2.5}$   
707 concentration. To control ACI-induced  $PM_{2.5}$  enhancement, first, a larger  
708 emission reduction is necessary in cloudy areas compared with less cloudy areas  
709 to bring about a noticeable decrease in ACI-induced LWP in response to  $PM_{2.5}$   
710 reduction. Second, secondary inorganic aerosol (SNA), which is an important  
711 component of total aerosol, has a large influence on the ACI-induced  $PM_{2.5}$   
712 enhancement because of its high hygroscopicity. This makes it easy for SNA to  
713 be activated as CCN and influence LWP. We think that it is crucial to make  
714 substantial decreases in the precursors of SNA, such as  $SO_2$ ,  $NO_x$  and  $NH_3$  species.  
715 These decreases could substantially decrease SNA. A large decrease in SNA  
716 would enhance the ACI-induced LWP response to  $PM_{2.5}$  reduction and cause a  
717 large decrease in ACI-induced  $PM_{2.5}$  enhancement. In addition, relative to ARI-  
718 induced  $PM_{2.5}$  enhancement, the lower decrease in ACI-induced  $PM_{2.5}$   
719 enhancement is mainly because of the small decrease in ACI-induced  
720 enhancements of secondary  $PM_{2.5}$  components. A substantial decrease in SNA  
721 would make the decrease ratio of ACI-induced  $PM_{2.5}$  enhancement approach the  
722 more rapid decrease ratio of ARI-induced  $PM_{2.5}$  enhancement.

Formatted: Font: (Default) Times New Roman

Formatted: Font: (Default) Times New Roman

Formatted: Font: (Default) Times New Roman

Formatted: Font: (Default) Times New Roman

Deleted: .

724

Formatted: Font: (Default) Times New Roman, 四号

Formatted: Normal

#### 725 **Data and Code availability.**

726 The data and code used in this study are available upon request from Da Gao  
727 (dagao94@foxmail.com).

728

#### 729 **Author Contribution**

730 D.G., B.Z. and S.W. designed the research; D.G., B.Z., J.S. and B.G. improved  
731 the WRF-Chem performance; D.G. and B.Z. further developed WRF-Chem and  
732 performed the simulations; X.W., S.L. and Z.D. provide the anthropogenic  
733 emissions; D.G. analyzed the data with the help from B.Z., S.W. and Y.W.; D.Y.  
734 and J.S. help D.G. to design some figures; S.W., Y.W., Y.Z. and Y.H. presented  
735 important suggestions for the analysis and writings; D.G. and B.Z. wrote the  
736 paper with inputs from all co-authors. \_

737

#### 738 **Competing interests**

739 The author declares no competing interests.

740

#### 741 **Acknowledgments.**

742 This research is supported by the National Key Research and Development  
743 Program of China (2022YFC3701000, Task 5), the National Natural Science  
744 Foundation of China (22188102), and the Tencent Foundation through the  
745 XPLOER PRIZE. We would like to thank Fenfen Zhang for providing the PM<sub>2.5</sub>

746 [components data for Handan city in January 2013.](#)

747

## 748 **References**

749 Abdul-Razzak H, Ghan SJ. A parameterization of aerosol activation - 3. Sectional  
750 representation. *J Geophys Res-Atmos* 2002, 107(D3).

751 Bellouin N, Quaas J, Gryspeerdt E, Kinne S, Stier P, Watson-Parris D, et al.  
752 Bounding Global Aerosol Radiative Forcing of Climate Change. *Rev*  
753 *Geophys* 2020, 58(1).

754 Bennartz R. Global assessment of marine boundary layer cloud droplet number  
755 concentration from satellite. *J Geophys Res-Atmos* 2007, 112(D2).

756 Bougeault P, Lacarrere P. Parameterization Of Orography-Induced Turbulence In  
757 a Mesobeta-Scale Model. *Mon Weather Rev* 1989, 117(8): 1872-1890.

758 Carter W. Documentation of the SAPRC-99 Chemical Mechanism for VOC  
759 Reactivity Assessment; 2000.

760 Ding AJ, Huang X, Nie W, Sun JN, Kerminen VM, Petaja T, et al. Enhanced haze  
761 pollution by black carbon in megacities in China. *Geophys Res Lett* 2016,  
762 43(6): 2873-2879.

763 Ding D, Xing J, Wang SX, Liu KY, Hao JM. Estimated Contributions of  
764 Emissions Controls, Meteorological Factors, Population Growth, and  
765 Changes in Baseline Mortality to Reductions in Ambient PM<sub>2.5</sub> and PM<sub>2.5</sub>-  
766 Related Mortality in China, 2013-2017. *Environ Health Persp* 2019, 127(6).

767 Donahue NM, Henry KM, Mentel TF, Kiendler-Scharr A, Spindler C, Bohn B, et

Formatted: Indent: Left: 0 cm, Hanging: 2 ch, First line:  
-2 ch

768 al. Aging of biogenic secondary organic aerosol via gas-phase OH radical  
769 reactions. *P Natl Acad Sci USA* 2012, 109(34): 13503-13508.

770 Emery C, Tai, E., Yarwood, G. . Enhanced meteorological modeling and  
771 performance evaluation for two texas episodes. Report to the Texas Natural  
772 Resources Conservation Commission; 2001.

773 Fan JW, Wang Y, Rosenfeld D, Liu XH. Review of Aerosol-Cloud Interactions:  
774 Mechanisms, Significance, and Challenges. *J Atmos Sci* 2016, 73(11): 4221-  
775 4252.

776 Fast JD, Gustafson WI, Easter RC, Zaveri RA, Barnard JC, Chapman EG, et al.  
777 Evolution of ozone, particulates, and aerosol direct radiative forcing in the  
778 vicinity of Houston using a fully coupled meteorology-chemistry-aerosol  
779 model. *J Geophys Res-Atmos* 2006, 111(D21).

780 Forkel R, Balzarini A, Baro R, Bianconi R, Curci G, Jimenez-Guerrero P, et al.  
781 Analysis of the WRF-Chem contributions to AQMEII phase2 with respect  
782 to aerosol radiative feedbacks on meteorology and pollutant distributions.  
783 *Atmos Environ* 2015, 115: 630-645.

784 Forkel R, Werhahn J, Hansen AB, McKeen S, Peckham S, Grell G, et al. Effect  
785 of aerosol-radiation feedback on regional air quality - A case study with  
786 WRF/Chem. *Atmos Environ* 2012, 53: 202-211.

787 Forster P, T. Storelvmo, K. Armour, W. Collins, J.-L. Dufresne, D. Frame, D.J.  
788 Lunt, T. Mauritsen, M.D. Palmer, M. Watanabe, M. Wild, and H. Zhang. The  
789 Earth's Energy Budget, Climate Feedbacks, and Climate Sensitivity. In

790 Climate Change 2021: The Physical Science Basis. Contribution of Working  
791 Group I to the Sixth Assessment Report of the Intergovernmental Panel on  
792 Climate Change [Masson-Delmotte, V., P. Zhai, A. Pirani, S.L. Connors, C.  
793 Péan, S. Berger, N. Caud, Y. Chen, L. Goldfarb, M.I. Gomis, M. Huang,  
794 K. Leitzell, E. Lonnoy, J.B.R. Matthews, T.K. Maycock, T. Waterfield, O.  
795 Yelekçi, R. Yu, and B. Zhou (eds.)]. Cambridge University Press: Cambridge,  
796 United Kingdom and New York, NY, USA; 2021.

797 Gao M, Han ZW, Tao ZN, Li JW, Kang JE, Huang K, et al. Air quality and climate  
798 change, Topic 3 of the Model Inter-Comparison Study for Asia Phase III  
799 (MICS-Asia III) - Part 2: aerosol radiative effects and aerosol feedbacks.  
800 Atmos Chem Phys 2020, 20(2): 1147-1161.

801 Gong W, Makar PA, Zhang J, Milbrandt J, Gravel S, Hayden KL, et al. Modelling  
802 aerosol-cloud-meteorology interaction: A case study with a fully coupled air  
803 quality model (GEM-MACH). Atmos Environ 2015, 115: 695-715.

804 Grell GA, Freitas SR. A scale and aerosol aware stochastic convective  
805 parameterization for weather and air quality modeling. Atmos Chem Phys  
806 2014, 14(10): 5233-5250.

807 Guenther A, Karl T, Harley P, Wiedinmyer C, Palmer PI, Geron C. Estimates of  
808 global terrestrial isoprene emissions using MEGAN (Model of Emissions of  
809 Gases and Aerosols from Nature). Atmos Chem Phys 2006, 6: 3181-3210.

810 Gustafson WI, Chapman EG, Ghan SJ, Easter RC, Fast JD. Impact on modeled  
811 cloud characteristics due to simplified treatment of uniform cloud

812 condensation nuclei during NEAQS 2004. *Geophys Res Lett* 2007, 34(19).

813 Hong CP, Zhang Q, Zhang Y, Davis SJ, Zhang X, Tong D, et al. Weakening  
814 aerosol direct radiative effects mitigate climate penalty on Chinese air  
815 quality. *Nat Clim Change* 2020, 10(9): 845-+.

816 Iacono MJ, Delamere JS, Mlawer EJ, Shephard MW, Clough SA, Collins WD.  
817 Radiative forcing by long-lived greenhouse gases: Calculations with the  
818 AER radiative transfer models. *J Geophys Res-Atmos* 2008, 113(D13).

819 Janjic ZI. The Step-Mountain Eta Coordinate Model - Further Developments Of  
820 the Convection, Viscous Sublayer, And Turbulence Closure Schemes. *Mon*  
821 *Weather Rev* 1994, 122(5): 927-945.

822 Kanji ZA, Ladino LA, Wex H, Boose Y, Burkert-Kohn M, Cziczo DJ, et al.  
823 Overview of Ice Nucleating Particles. *Meteor Mon* 2017, 58.

824 Kong X, Forkel R, Sokhi RS, Suppan P, Baklanov A, Gauss M, et al. Analysis of  
825 meteorology-chemistry interactions during air pollution episodes using  
826 online coupled models within AQMEII phase-2. *Atmos Environ* 2015, 115:  
827 527-540.

828 Le TH, Wang Y, Liu L, Yang JN, Yung YL, Li GH, et al. Unexpected air pollution  
829 with marked emission reductions during the COVID-19 outbreak in China.  
830 *Science* 2020, 369(6504): 702-+.

831 Li L, An JY, Zhou M, Yan RS, Huang C, Lu Q, et al. Source apportionment of  
832 fine particles and its chemical components over the Yangtze River Delta,  
833 China during a heavy haze pollution episode. *Atmos Environ* 2015, 123:

834 415-429.

835 Li M, Zhang Q, Kurokawa J, Woo JH, He KB, Lu ZF, et al. MIX: a mosaic Asian  
836 anthropogenic emission inventory under the international collaboration  
837 framework of the MICS-Asia and HTAP. *Atmos Chem Phys* 2017, 17(2):  
838 935-963.

839 Li Shengyue WS, Wu Qingru. Emission trends of air pollutants and CO<sub>2</sub> in China  
840 from 2005 to 2021. *Earth System Science Data* 2023.

841 Lin CJ. Characteristics and Sources of Water-soluble Inorganic Ions in  
842 Atmospheric Particulate Matter and Rainfall in the suburb of Mianyang.  
843 Master thesis, Southwest University of Science and Technology, 2022.

844 Liu Q, Jia XC, Quan JN, Li JY, Li X, Wu YX, et al. New positive feedback  
845 mechanism between boundary layer meteorology and secondary aerosol  
846 formation during severe haze events. *Sci Rep-Uk* 2018, 8.

847 Liu S, Xing J, Zhao B, Wang JD, Wang SX, Zhang XY, et al. Understanding of  
848 Aerosol-Climate Interactions in China: Aerosol Impacts on Solar Radiation,  
849 Temperature, Cloud, and Precipitation and Its Changes Under Future  
850 Climate and Emission Scenarios. *Curr Pollut Rep* 2019, 5(2): 36-51.

851 Liu YY, Xing J, Wang SX, Fu X, Zheng HT. Source-specific speciation profiles  
852 of PM<sub>2.5</sub> for heavy metals and their anthropogenic emissions in China.  
853 *Environ Pollut* 2018, 239: 544-553.

854 Matthias V, Aulinger A, Bieser J, Chen YJ, Geyer B, Gao J, et al. Modeling high  
855 aerosol loads in China in January 2013. *Urban Clim* 2017, 22: 35-50.



856 Moch JM, Mickley LJ, Keller CA, Bian HS, Lundgren EW, Zhai SX, et al.  
857 Aerosol-Radiation Interactions in China in Winter: Competing Effects of  
858 Reduced Shortwave Radiation and Cloud-Snowfall-Albedo Feedbacks  
859 Under Rapidly Changing Emissions. *J Geophys Res-Atmos* 2022, 127(9).

860 Morrison H, Thompson G, Tatarskii V. Impact of Cloud Microphysics on the  
861 Development of Trailing Stratiform Precipitation in a Simulated Squall Line:  
862 Comparison of One- and Two-Moment Schemes. *Mon Weather Rev* 2009,  
863 137(3): 991-1007.

864 Myhre G, Stordal F, Johnsrud M, Kaufman YJ, Rosenfeld D, Storelvmo T, et al.  
865 Aerosol-cloud interaction inferred from MODIS satellite data and global  
866 aerosol models. *Atmos Chem Phys* 2007, 7(12): 3081-3101.

867 Niu GY, Yang ZL, Mitchell KE, Chen F, Ek MB, Barlage M, et al. The community  
868 Noah land surface model with multiparameterization options (Noah-MP): 1.  
869 Model description and evaluation with local-scale measurements. *J Geophys*  
870 *Res-Atmos* 2011, 116.

871 Rosenfeld D, Sherwood S, Wood R, Donner L. Climate Effects of Aerosol-Cloud  
872 Interactions. *Science* 2014, 343(6169): 379-380.

873 Savane OS, Vant-Hull B, Mahani S, Khanbilvardi R. Effects of Aerosol on Cloud  
874 Liquid Water Path: Statistical Method a Potential Source for Divergence in  
875 Past Observation Based Correlative Studies. *Atmosphere-Basel* 2015, 6(3):  
876 273-298.

877 Seinfeld JH, Bretherton C, Carslaw KS, Coe H, DeMott PJ, Dunlea EJ, et al.

878 Improving our fundamental understanding of the role of aerosol-cloud  
879 interactions in the climate system. *P Natl Acad Sci USA* 2016, 113(21):  
880 5781-5790.

881 Shrivastava M, Fast J, Easter R, Gustafson WI, Zaveri RA, Jimenez JL, et al.  
882 Modeling organic aerosols in a megacity: comparison of simple and  
883 complex representations of the volatility basis set approach. *Atmos Chem*  
884 *Phys* 2011, 11(13): 6639-6662.

885 Wang H, Shi GY, Zhang XY, Gong SL, Tan SC, Chen B, et al. Mesoscale  
886 modelling study of the interactions between aerosols and PBL meteorology  
887 during a haze episode in China Jing-Jin-Ji and its near surrounding region -  
888 Part 2: Aerosols' radiative feedback effects. *Atmos Chem Phys* 2015, 15(6):  
889 3277-3287.

890 Wang JD, Wang SX, Jiang JK, Ding AJ, Zheng M, Zhao B, et al. Impact of  
891 aerosol-meteorology interactions on fine particle pollution during China's  
892 severe haze episode in January 2013. *Environ Res Lett* 2014, 9(9).

893 Wang JD, Zhao B, Wang SX, Yang FM, Xing J, Morawska L, et al. Particulate  
894 matter pollution over China and the effects of control policies. *Sci Total*  
895 *Environ* 2017, 584: 426-447.

896 Wang LW, Wen L, Xu CH, Chen JM, Wang XF, Yang LX, et al. HONO and its  
897 potential source particulate nitrite at an urban site in North China during the  
898 cold season. *Sci Total Environ* 2015, 538: 93-101.

899 Wang YS, Li WJ, Gao WK, Liu ZR, Tian SL, Shen RR, et al. Trends in particulate

900 matter and its chemical compositions in China from 2013-2017. *Sci China*  
901 *Earth Sci* 2019, 62(12): 1857-1871.

902 Wang ZF, Li, J., Wang, Z., Yang, W., Tang, X., Ge, B., Yan, P., Zhu, L., Chen, X.,  
903 and Chen, H. Modeling study of regional severe hazes over mid-eastern  
904 China in January 2013 and its implications on pollution prevention and  
905 control. *Science China Earth Sciences* 2014(57): 3-13.

906 Wild O, Zhu X, Prather MJ. Fast-j: Accurate simulation of in- and below-cloud  
907 photolysis in tropospheric chemical models. *J Atmos Chem* 2000, 37(3):  
908 245-282.

909 Wu JR, Bei NF, Hu B, Liu SX, Wang Y, Shen ZX, et al. Aerosol-photolysis  
910 interaction reduces particulate matter during wintertime haze events. *P Natl*  
911 *Acad Sci USA* 2020, 117(18): 9755-9761.

912 Xiong CR, Li J, Liu ZX, Zhang ZY. The dominant role of aerosol-cloud  
913 interactions in aerosol-boundary layer feedback: Case studies in three  
914 megacities in China. *Front Env Sci-Switz* 2022, 10.

915 Xue CY, Zhang CL, Ye C, Liu PF, Catoire V, Krysztofiak G, et al. HONO Budget  
916 and Its Role in Nitrate Formation in the Rural North China Plain. *Environ*  
917 *Sci Technol* 2020, 54(18): 11048-11057.

918 Zaveri RA, Easter RC, Fast JD, Peters LK. Model for Simulating Aerosol  
919 Interactions and Chemistry (MOSAIC). *J Geophys Res-Atmos* 2008,  
920 113(D13).

921 Zhang B, Wang Y, Hao J. Simulating aerosol-radiation-cloud feedbacks on

922 meteorology and air quality over eastern China under severe haze conditions  
923 in winter. *Atmos Chem Phys* 2015, 15(5): 2387-2404.

924 Zhang F, Wang Y, Peng JF, Chen L, Sun YL, Duan L, et al. An unexpected catalyst  
925 dominates formation and radiative forcing of regional haze. *P Natl Acad Sci*  
926 USA 2020, 117(8): 3960-3966.

927 Zhang FF. Characteristics of Air Pollution and Chemical Composition of PM2.5  
928 in Handan Master thesis, Hebei University of Engineering, 2015.

929 Zhang FF, Xing J, Ding DA, Wang JD, Zheng HT, Zhao B, et al. Role of black  
930 carbon in modulating aerosol direct effects driven by air pollution controls  
931 during 2013-2017 in China. *Sci Total Environ* 2022, 832.

932 Zhang X, Zhang Q, Hong CP, Zheng YX, Geng GN, Tong D, et al. Enhancement  
933 of PM2.5 Concentrations by Aerosol-Meteorology Interactions Over China.  
934 *J Geophys Res-Atmos* 2018, 123(2): 1179-1194.

935 Zhao B, Liou KN, Gu Y, Li QB, Jiang JH, Su H, et al. Enhanced PM2.5 pollution  
936 in China due to aerosol-cloud interactions. *Sci Rep-Uk* 2017, 7.

937 Zhao C, Chen S, Leung LR, Qian Y, Kok JF, Zaveri RA, et al. Uncertainty in  
938 modeling dust mass balance and radiative forcing from size parameterization.  
939 *Atmos Chem Phys* 2013, 13(21): 10733-10753.

940 Zhao C, Liu X, Leung LR, Johnson B, McFarlane SA, Gustafson WI, et al. The  
941 spatial distribution of mineral dust and its shortwave radiative forcing over  
942 North Africa: modeling sensitivities to dust emissions and aerosol size  
943 treatments. *Atmos Chem Phys* 2010, 10(18): 8821-8838.

- 944 Zheng HT, Cai SY, Wang SX, Zhao B, Chang X, Hao JM. Development of a unit-  
945 based industrial emission inventory in the Beijing-Tianjin-Hebei region and  
946 resulting improvement in air quality modeling. *Atmos Chem Phys* 2019,  
947 19(6): 3447-3462.
- 948 Zhou M, Zhang L, Chen D, Gu Y, Fu TM, Gao M, et al. The impact of aerosol-  
949 radiation interactions on the effectiveness of emission control measures.  
950 *Environ Res Lett* 2019, 14(2).